Journal of Catalysis **195,** 51–61 (2000)
doi:10.1006/jcat.2000.2990, available online at http://www.idealibrary.com on IDEAL®

Performance and Characterization of a New Crystalline $SbRe_2O_6$ Catalyst for Selective Oxidation of Methanol to Methylal

Youzhu Yuan,[1] Haichao Liu, Hideo Imoto, Takafumi Shido, and Yasuhiro Iwasawa[2]

Department of Chemistry, Graduate School of Science, The University of Tokyo, Hongo, Bunkyo-ku, Tokyo 113-0033, Japan

Received February 29, 2000; revised June 26, 2000; accepted July 14, 2000

Three well-defined compounds, $SbRe_2O_6$, $Sb_4Re_2O_{13}$, and $SbOReO_4 \cdot 2H_2O$, and several supported Re catalysts were employed as catalysts for the selective oxidation of methanol to methylal ($3CH_3OH + 1/2O_2 \rightarrow CH_2(OCH_3)_2 + 2H_2O$). High selectivity of 92.5% to methylal was obtained on the new crystalline catalyst $SbRe_2O_6$ at 573 K, while no methylal formation or negligible activity was observed with the other catalysts. No structural change in the bulk and surface of the $SbRe_2O_6$ catalyst occurred after the methanol oxidation below 600 K as characterized by XRD, Raman, XPS, and SEM. The reaction rate increased with increasing methanol partial pressure, while the selectivity to methylal was independent of methanol partial pressure as well as O_2 partial pressure (<10 mol%). There existed two types of active lattice oxygen species in TPD experiments on $SbRe_2O_6$, both being responsible for the methylal formation. The high performance of $SbRe_2O_6$ for the selective synthesis of methylal from methanol may be ascribed to the Re–oxide species stabilized by the specific connection with Sb oxides at the crystal surface.

Key Words: **Sb–Re–O mixed oxide catalysts; $SbRe_2O_6$; selective catalytic oxidation of methanol; methylal synthesis; XRD; XPS; Raman; SEM; TPD; TPR.**

1. INTRODUCTION

Numerous efforts have been made with the development of selective oxidation catalysts for methanol conversion to formaldehyde, methyl formate, or dimethoxymethane (methylal) from both academic and industrial interests. The methanol oxidation to formaldehyde has been extensively studied and commercialized on silver and ferric molybdate catalysts (1). Methyl formate has also been produced with high yields by the catalytic oxidation of methanol on V–Ti oxides (2), Sn–Mo oxides (3), and Bi-based mixed oxides (4). However, methylal, which is used as a gasoline additive, a solvent in the perfume industry, a key intermediate for preparing high-concentration formaldehyde, and a reagent in organic synthesis, has not successfully been produced by catalytic methanol oxidation. The catalytic methylal synthesis from methanol has been reported on V/TiO_2 (2), V–Mo–O (5), PMoH-5.75/SiO_2 (6), Mo/MCM-41 (7), a MoO_3(100) plane (8), and electrocatalysts (9), but the selectivities to methylal on those catalysts were low and practically insignificant. Hence, discovery of a new selective oxidation catalyst is the key issue to realizing the direct methylal synthesis from methanol, where three methanol molecules are incorporated into a methylal molecule.

We have examined combinations of Sb and Re oxides as selective oxidation catalysts (10, 11). The occurrence of rhenium in a wide range of oxidation states leads to a rich and interesting chemistry that is illustrated in both binary and ternary oxides (12–17). Supported rhenium oxide catalysts are active for alkene metathesis (18, 19) and hydrodesulfurization (HDS) of heavy fractions of crude oil (20, 21). For these reactions supported rhenium oxide catalysts exhibit activities superior to supported molybdenum and tungsten oxide catalysts. Up to date, there are no rhenium oxide catalysts that work efficiently in selective methanol oxidation due to facile volatilization of rhenium oxide species formed during catalyst pretreatments and under the reaction conditions (12, 22–27). Meanwhile, antimony is a well-known promoter element in selective oxidation catalysts, providing many mixed oxide formulations together with V, Sn, Mo, Fe, and U (27–32). We reported good performances of a Pt/SbO_x catalyst for the selective oxidation of isobutane and isobutylene to methacrolein (33, 34). On the Pt/SbO_x catalyst, a Sb_6O_{13} phase formed *in situ* under the catalytic reaction conditions contributes to the selective performance. The Sb_6O_{13} has a defect pyrochlore-type cubic structure, consisting of a network of SbO_6 octahedra with $-Sb^{3+}-O^{2-}-$ chains positioned inside vacancies formed by the network of octahedra (35). A new crystalline compound, $SbRe_2O_6$, has similar $Sb^{3+}-O^{2-}$ chains that connect with $[Re_2O_6]^{3-}$ layers (14).

Recently, we have found that three Sb–Re–O crystalline oxides, $SbOReO_4 \cdot 2H_2O$, $Sb_4Re_2O_{13}$, and particularly $SbRe_2O_6$, constitute a new family of promising catalysts

[1] Permanent address: Department of Chemistry, State Key Laboratory for Physical Chemistry of Solid Surface, Xiamen University, Xiamen 361005, China.

[2] To whom correspondence should be addressed. E-mail: iwasawa@chem.s.u-tokyo.ac.jp. Fax: 81-3-5800-6892.

0021-9517/00 $35.00

for the selective oxidation reactions of isobutane and isobutylene at 673–773 K (10, 11). The detailed characterizations of the crystalline oxides by XPS, Raman, SEM, and XRD, however, revealed that there was a significant decomposition of the Sb–Re–O compounds during the catalytic selective oxidation of isobutane at 773 K (10, 11).

More recently, we have discovered that the selective catalytic oxidation of methanol to methylal efficiently proceeds on $SbRe_2O_6$ with a selectivity as high as 92.5% at 573 K, in which there is no structural change in the $SbRe_2O_6$ crystal (36). The aim of this paper is to discuss the key issues relevant to the good performance of the new $SbRe_2O_6$ catalyst for the selective oxidation of methanol to methylal by means of flow and pulse experiments, XRD, XPS, Raman, SEM, TPD, and TPR.

2. EXPERIMENTAL

2.1. Catalyst Preparation

Three well-defined Re–Sb–O compounds, $SbOReO_4 \cdot 2H_2O$, $SbRe_2O_6$, and $Sb_4Re_2O_{13}$, were prepared according to the procedures reported previously (10–14). Sb_2O_3 (Soekawa, purity 99.99%) and SiO_2 (Aerosil 200) were used as supports for Re oxides. The supported Re oxides were prepared by an incipient wetness impregnation method using an aqueous NH_4ReO_4 (Soekawa, purity 99.9%) solution. A mechanical mixture catalyst of Sb_2O_3 with NH_4ReO_4 was also prepared by the known method (37). The decomposition of the ammonium perrhenate precursor to Re_2O_7 in the supported samples and the mechanically mixed sample was performed by temperature-programmed calcination (4 K/min) up to 573 K in a flow of $He/O_2 =$ 90.0/10.0 (mol%) at atmospheric pressure and the samples were further calcined at 573 K for 2 h. They are denoted as Re_2O_7/Sb_2O_3, Re_2O_7/SiO_2, and $Re_2O_7 + Sb_2O_3$, respectively.

2.2. Catalytic Methanol Oxidation

The catalytic performances were examined in a conventional fixed-bed flow reactor by using 200 mg of catalyst at 1 atm. All the catalysts were pretreated under He at 573 K for 1 h *in situ* before catalytic reaction. These samples are denoted as "fresh" ones. Methanol (Wako, purity 99.8%) was introduced to the flow reactor by bubbling He gas through a glass saturator filled with methanol. The reactant mixture of $He/O_2/MeOH$ was adjusted to 86.3/9.7/4.0 (mol%) or 79.3/9.7/10.0 (mol%) by mass flow controllers. The typical performances were conducted at $GHSV = 10{,}000\ ml\ h^{-1}\ g_{cat}^{-1}$. The outlet stream line from the reactor to the gas chromatgraph was heated at about 423 K to avoid condensation of reaction products. The products were analyzed with an on-line gas chromatgraph using two columns (3-m Porapak N and 3-m Unibeads C) at 423 K.

Pulse experiments were carried out in the same system by using He as the carrier gas in a flow rate of 60 ml/min. The catalyst $SbRe_2O_6$ (200 mg) was pretreated at 573 K under He for 1 h. The amount of ca. 1 ml of $He/MeOH = 96.0/4.0$ (mol%) was pulsed into the catalyst bed at 573 K at an interval of about 15 min. The effluent gas from the reactor was analyzed by the on-line gas chromatgraph.

2.3. Characterization

The Re–Sb–O catalysts were characterized *ex situ* before and after selective methanol oxidation by powder X-ray diffraction (XRD), X-ray photoelectron spectroscopy (XPS), scanning electron microscopy (SEM), and Mircroconfocal laser Raman spectroscopy (Raman). In addition, the samples were characterized by O_2 temperature-programmed desorption (TPD) and H_2 temperature-programmed reduction (TPR).

XRD patterns were measured on a Rigaku Miniflex goniometer. The analysis was carried out in a continuous $\theta/2\theta$ scan reflection mode using Cu $K\alpha$ radiation ($\lambda = 0.15418$). The anode was operated at 30 kV and 15 mA. The 2θ angles were scanned from 5° to 60° at a rate of 2°/min.

Raman spectra were recorded under an ambient atmosphere by using a confocal microprobe Raman system (LabRam I). A holographic notch filter was equipped to filter the excitation line and an 1800 g mm^{-1} holographic grating was employed to disperse the scattered light. The excitation wavelength was 632.8 nm with a power of 12 mW from an internal He–Ne laser. The size focused on the sample surface was ca. 5 μm.

XPS spectra were measured on a Rigaku XPS-7000 spectrometer by using Mg $K\alpha$ radiation (1253.6 eV) with X-ray power of 200 W (accelerating voltage, 20 kV; emission current, 10 mA). Samples were pressed into thin disks, placed on holders, outgassed to less than 2.6×10^{-5} Pa in a prechamber, and transferred to an analysis chamber. The binding energy was referred to 284.6 eV for C 1*s*. The peak intensity was normalized by the peak height of Sb 4*d* at 34.4 eV. The peak deconvolution and fitting was performed by using a software of SpXzeigR2.1 running with IgorPro and Gaussian–Lorentzian lineshape, fixing both spin–orbit splitting and the relative intensity of spin–orbit components.

SEM images were taken on a Hitachi S-4500 microscope equipped with a field emission gun operated with an acceleration voltage of 5 kV and an emission current of 10 μA. The samples were imaged without any metallic coating. The SEM micrographs were taken at many different places of the sample.

TPD spectra were measured in a fixed-bed reactor system equipped with a gas chromatograph. A dry-ice/acetone trap was used to eliminate the influence of water and hydrocarbons. $SbRe_2O_6$ was pretreated at 573 K for 1 h and then cooled to 298 K in He. The O_2 adsorption was carried

out at 298 K under He/O_2 (90/10, molar ratio) in a flow of 30 ml/min for 10 min. The sample was purged by a He flow (40 ml/min) for 60 min. Then, O_2-TPD spectra were measured at a heating rate of 10 K/min.

TPR spectra were recorded in the same fixed-bed reaction system as that for TPD. Again, a dry-ice/acetone trap was used to eliminate the influences of water and hydrocarbons. The samples were exposed to Ar flow for 2 h at room temperature and to a 5% H_2/Ar flow of 30 ml/min. The TPR spectra were recorded at a heating rate of 10 K/min.

3. RESULTS

3.1. Methanol Oxidation on Sb–Re–O Catalysts

The performances of several Sb–Re–O catalysts at 573 K for the methanol conversion to methylal are shown in Table 1. Sb oxides such as Sb_2O_3, Sb_2O_4, and Sb_2O_5, a mechanical mixture of Sb_2O_3 and Re_2O_7 ($Re_2O_7 + Sb_2O_3$), and Re oxides supported on Sb_2O_3 and SiO_2 (Re_2O_7/Sb_2O_3 and Re_2O_7/SiO_2, respectively) showed no or negligible activities for the methylal formation. The crystalline Sb–Re oxides, $Sb_4Re_2O_{13}$ and $SbOReO_4 \cdot 2H_2O$, produced almost no methylal either. Only $SbRe_2O_6$ among the crystalline Sb–Re oxides synthesized thus far was active for selective methanol oxidation to methylal. The methylal selectivity was as high as 92.5% at a conversion of 6.5% at 573 K (Table 1).

Figure 1 shows the reaction rate and selectivity for catalytic methylal synthesis on $SbRe_2O_6$ under GHSV = 10,000 mol h^{-1} g_{cat}^{-1} and $He/O_2/MeOH = 86.3/9.7/4.0$ (mol%) as a function of reaction temperature. The

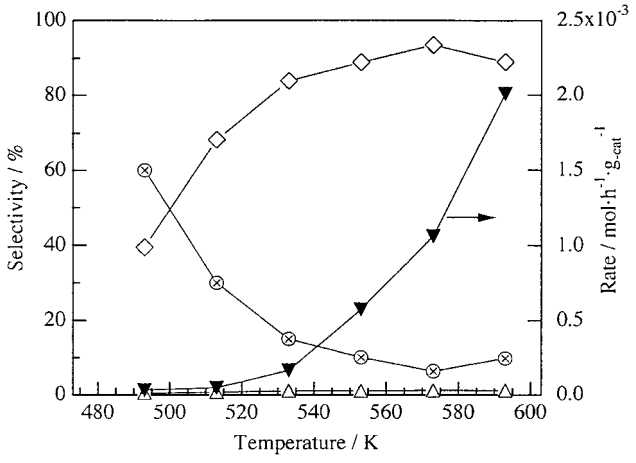

FIG. 1. Catalytic methanol oxidation on $SbRe_2O_6$ as a function of reaction temperature; GHSV = 10,000 ml h^{-1} g_{cat}^{-1}; $He/O_2/MeOH = 86.3/9.7/4.0$ (mol%); 1 atm. ◇, methylal selectivity; ⊗, dimethyl ether selectivity; △, methyl formate selectivity; ▼, reaction rate.

100% conversion of methanol corresponds to a reaction rate of 16.4×10^{-3} mol h^{-1} g_{cat}^{-1}. The reaction rate and methylal selectivity increased with increasing temperature up to 573 K, where the selectivity to methylal reached a maximum of 92.5%. A main by-product was dimethyl ether, whose formation decreased with increasing temperatures. The lower the GHSV, the higher the methanol conversion became, while selectivity to methylal was almost independent of the GHSV.

To check the catalytic performances of the three crystalline Sb–Re–O compounds at higher temperatures, we

TABLE 1

Methanol Oxidation over Several Sb–Re–O Catalysts at 573 K and on Other Typical Catalysts for Comparison

Catalyst	Conv. (%)	Selectivity (%)							Ref.
		$CH_2(OCH_3)_2$	HCHO	CH_3OCH_3	$HCOOCH_3$	HCOOH	CO_2	CO	
$SbRe_2O_6$[b]	6.5	92.5	0	6.3	1.2	0	0	0	This work
$Sb_4Re_2O_{13}$[b]	0	0	0	0	0	0	0	0	This work
$SbOReO_4 \cdot 2H_2O$[b]	4.7	1.0	0	99.0	0	0	0	0	This work
Re_2O_7/Sb_2O_3	2.5	7.4	49.8	42.7	0	0	0	0	This work
Re_2O_7/SiO_2	25.5	19.1	0	0.9	1.4	31.5	45.2	1.9	This work
$Re_2O_7 + Sb_2O_3$	1.4	23.6	0	76.4	0	0	0	0	This work
Sb_2O_3	0	0	0	0	0	0	0	0	This work
Sb_2O_4	0	0	0	0	0	0	0	0	This work
Sb_2O_5	1.3	Trace	55.5	26.4	0	0	18.0	0	This work
$PMoH\text{-}5.75/SiO_2$[c]	—	~56	~17	~7	~20	0	0	0	6
2mol%Mo/MCM-41[d]	0.7	76.2	0	23.8	0	0	0	0	7
V/TiO_2[e]	—	40	60	0	0	0	0	0	1

[a] Catalyst weight: 200 mg, pretreated under He at 573 K for 1 h before reaction. Reactant mixture: $He/O_2/MeOH = 86.3/9.7/4.0$ (mol%), GHSV = 10,000 ml h^{-1} g_{cat}^{-1}.

[b] Surface area = 1.0 m^2/g; reaction rate for $SbRe_2O_6 = 1.06 \times 10^{-3}$ mol h^{-1} g_{cat}^{-1}.

[c] Reaction temperature = 593 K; reactant mixture: $He/O_2/CH_3OH = 85.2/10.3/4.5$ (mol%). Reaction rate = 0.52 mol h^{-1} g_{Mo}^{-1}.

[d] Reaction temperature = 503 K; reactant mixture: $He/O_2/CH_3OH = 76.0/16.3/7.7$ (mol%). Reaction rate = 0.74×10^{-3} ml h^{-1} g_{cat}^{-1}.

[e] Reaction temperature = 473 K; reactant mixture: $He/O_2/CH_3OH = 76/16.3/7.7$ (mol%). Reaction rate = 0.035 ml h^{-1} g_{cat}^{-1}.

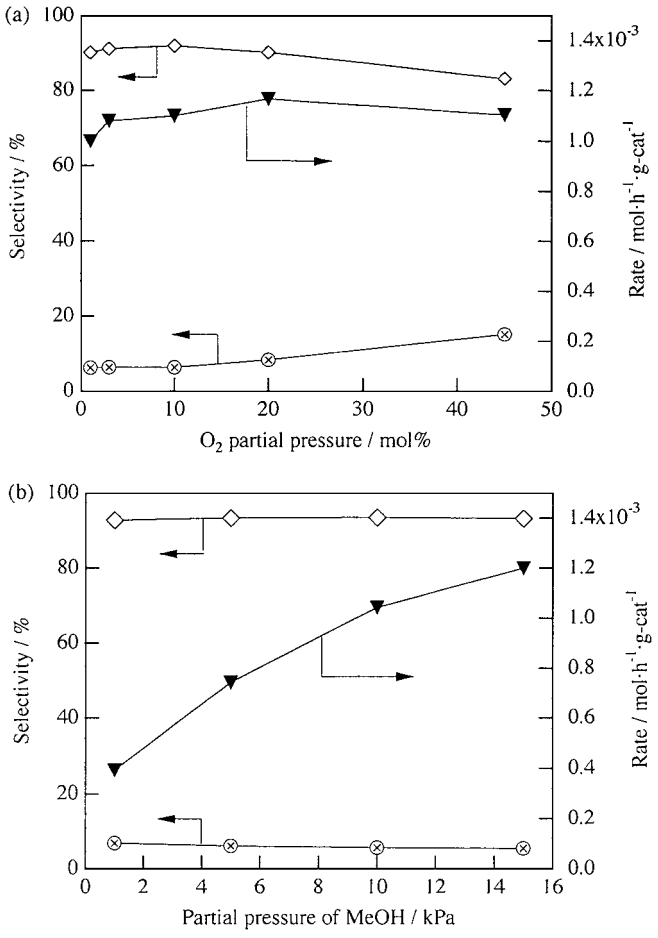

FIG. 2. (a) Catalytic methanol oxidation on $SbRe_2O_6$ as a function of oxygen partial pressure (MeOH = 15.0 mol% in the reactant feed). Reaction temperature = 573 K; GHSV = 5000 ml h^{-1} g^{-1}_{cat}. ▼, reaction rate; ◇, methylal selectivity; ⊗, dimethyl ether selectivity. (b) Catalytic methanol oxidation on $SbRe_2O_6$ as a function of methanol partial pressure (O_2 = 9.7 mol% in the reactant feed). Reaction temperature = 573 K; GHSV = 5000 ml h^{-1} g^{-1}_{cat}. ▼, reaction rate; ◇, methylal selectivity; ⊗, dimethyl ether selectivity.

examined the conversion and selectivity at 673 K. It was found that methanol conversion on $SbRe_2O_6$ at 673 K increased to 86.2%, keeping a high selectivity of 85.4% toward methylal. The performances of $Sb_4Re_2O_{13}$ and $SbOReO_4 \cdot 2H_2O$ were also improved to show 8.5% conversion with 60.1% selectivity and 8.7% conversion with 53.0% selectivity, respectively.

3.2. *Effects of O_2 and MeOH Pressures*

Figures 2a and 2b show reaction rates and selectivities for the methanol selective oxidation on $SbRe_2O_6$ at 573 K as a function of O_2 partial pressure and methanol partial pressure, respectively. The reaction rate was almost independent of O_2 partial pressure. The selectivity to methylal was kept constant at about 92–93% in the O_2 pressure range lower than 10 mol% in the reactant feed. When the O_2 pressure increased more, the selectivity decreased eventually to 84.0% at the 42 mol% O_2 pressure, accompanied by an increase in the dimethyl ether formation. The increase in the concentration of methanol resulted in the increase in the reaction rate. The selectivity to methylal was independent of the concentration of methanol.

3.3. *Effects of Gaseous O_2 on Methanol Oxidation*

In methanol conversion on $SbRe_2O_6$ at 573 K in the absence of O_2, methylal was the only detectable product with a selectivity of 100% in the effluent gas in the beginning of the reaction and methanol conversion rapidly decreased with time on stream. Then, methylal was not detected as a main product, and instead, H_2, CO_2, CH_4, and $HCOOCH_3$ were mainly produced. Note that the product ratio of $H_2/CO_2/CH_4$ after 2 h was close to 2/1/1 (molar ratio).

Figure 3 shows methanol oxidation on $SbRe_2O_6$ at 573 K in the absence of O_2 for 70 min and then in the presence of O_2. After the methanol conversion dropped to nearly zero, oxygen was introduced into the reactant feed, resulting in the recovery of the activity and methylal selectivity to the level similar to that at the steady-state reaction.

3.4. *Pulse Reaction*

The pulses of ca. 1 ml of He/MeOH = 96.0/4.0 (mol%) were introduced onto $SbRe_2O_6$ at 573 K at an interval of

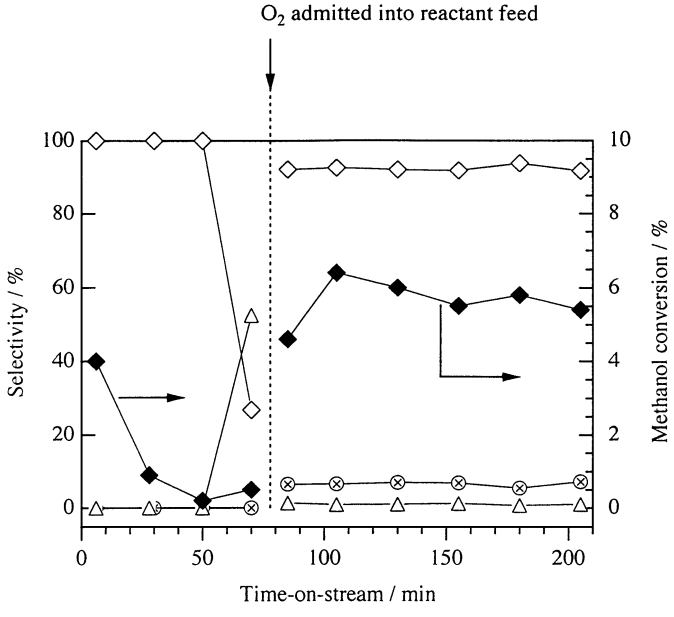

FIG. 3. Catalytic methanol oxidation on $SbRe_2O_6$ at 573 K as a function of time on stream. GHSV = 5000 ml h^{-1} g^{-1}_{cat}; He/MeOH = 90.0/10.0 (mol%) for 70 min and then He/O_2/MeOH = 79.3/9.7/10.0 (mol%). ◆, methanol conversion; ◇, methylal selectivity; ⊗, dimethyl ether selectivity; △, methyl formate selectivity.

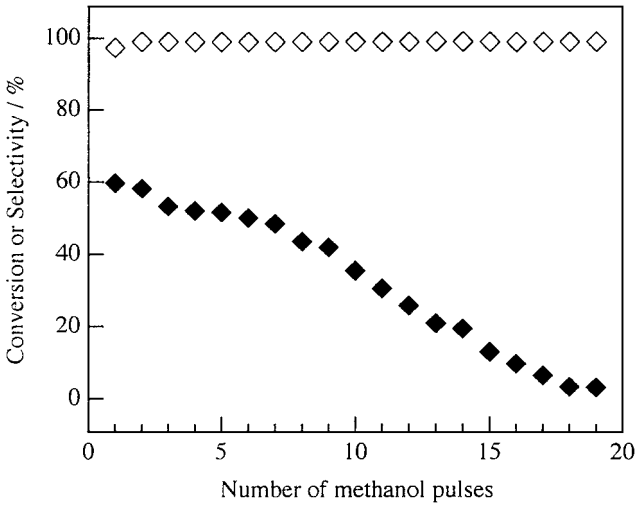

FIG. 4. Methanol pulse reactions on $SbRe_2O_6$ at 573 K. ◆, methanol conversion; ◇, methylal selectivity.

about 15 min. Figure 4 is the plots of the methanol conversion and the selectivity to methylal versus the number of methanol pulses. The selectivity to methylal was as high as 99.0% throughout the 19 pulses, which reproduces the results of the catalytic oxidation of methanol in the absence of oxygen in Fig. 3. The methanol conversion decreased with an increase in the number of pulses, passed a plateau from the fourth pulse to the seventh pulse, and decreased notably with increasing pulses.

3.5. Characterization by XRD, XPS, Raman, and SEM

Figure 5 depicts the XRD patterns of the $SbRe_2O_6$ catalyst before and after the catalytic methanol oxidation at 573, 593, and 673 K. The XRD patterns of the fresh $SbRe_2O_6$ and the $SbRe_2O_6$ after the catalytic reactions at 573 and 593 K were similar to each other. But there existed an additional broad diffraction peak at $2\theta \approx 31^\circ$ for the $SbRe_2O_6$ catalyst after the reaction at 673 K.

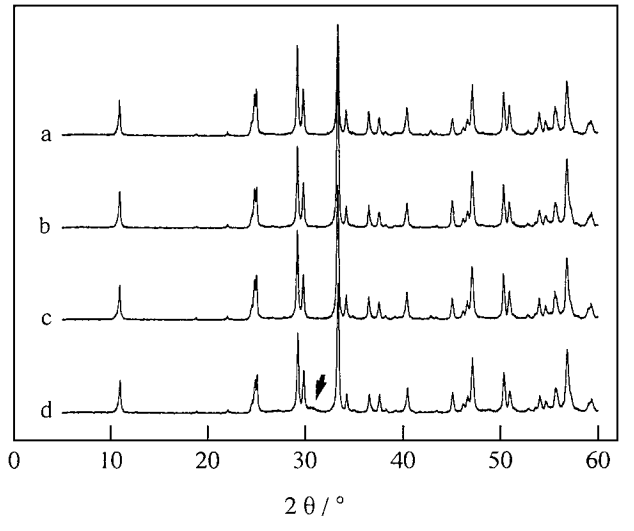

FIG. 5. XRD patterns for fresh $SbRe_2O_6$ (a), $SbRe_2O_6$ after the methanol oxidation at 573 K for 1 h (b), $SbRe_2O_6$ after the methanol oxidation at 593 K for 1 h (c), and $SbRe_2O_6$ after the methanol oxidation at 673 K for 3 h (d).

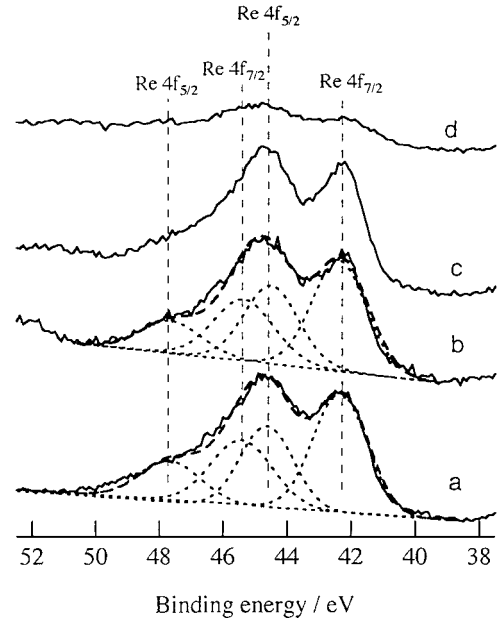

FIG. 6. XPS spectra for fresh $SbRe_2O_6$ (a), $SbRe_2O_6$ after the methanol oxidation at 573 K for 1 h (b), $SbRe_2O_6$ after the methanol oxidation at 593 K for 1 h (c), and $SbRe_2O_6$ after the methanol oxidation at 673 K for 3 h (d).

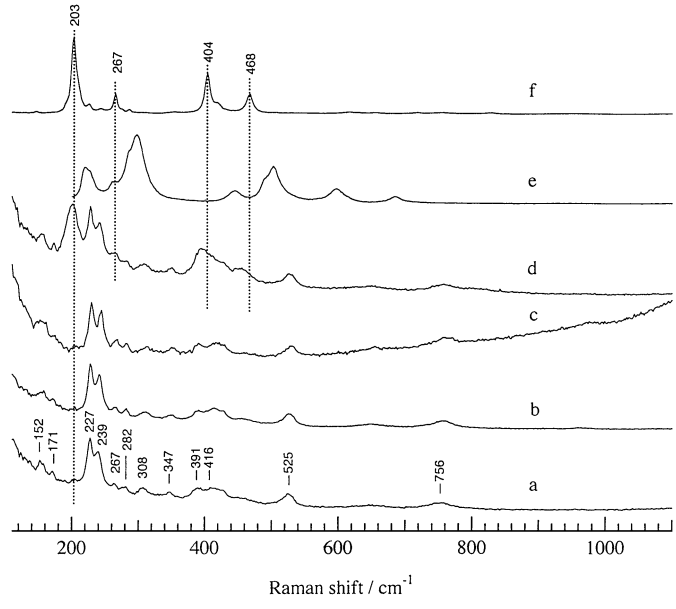

FIG. 7. Confocal laser Raman spectra for fresh $SbRe_2O_6$ (a), $SbRe_2O_6$ after the methanol oxidation at 573 K for 1 h (b), $SbRe_2O_6$ after the methanol oxidation at 593 K for 1 h (c), and $SbRe_2O_6$ after the methanol oxidation at 673 K for 3 h (d); Sb_2O_3 (e) and Sb_2O_4 (f).

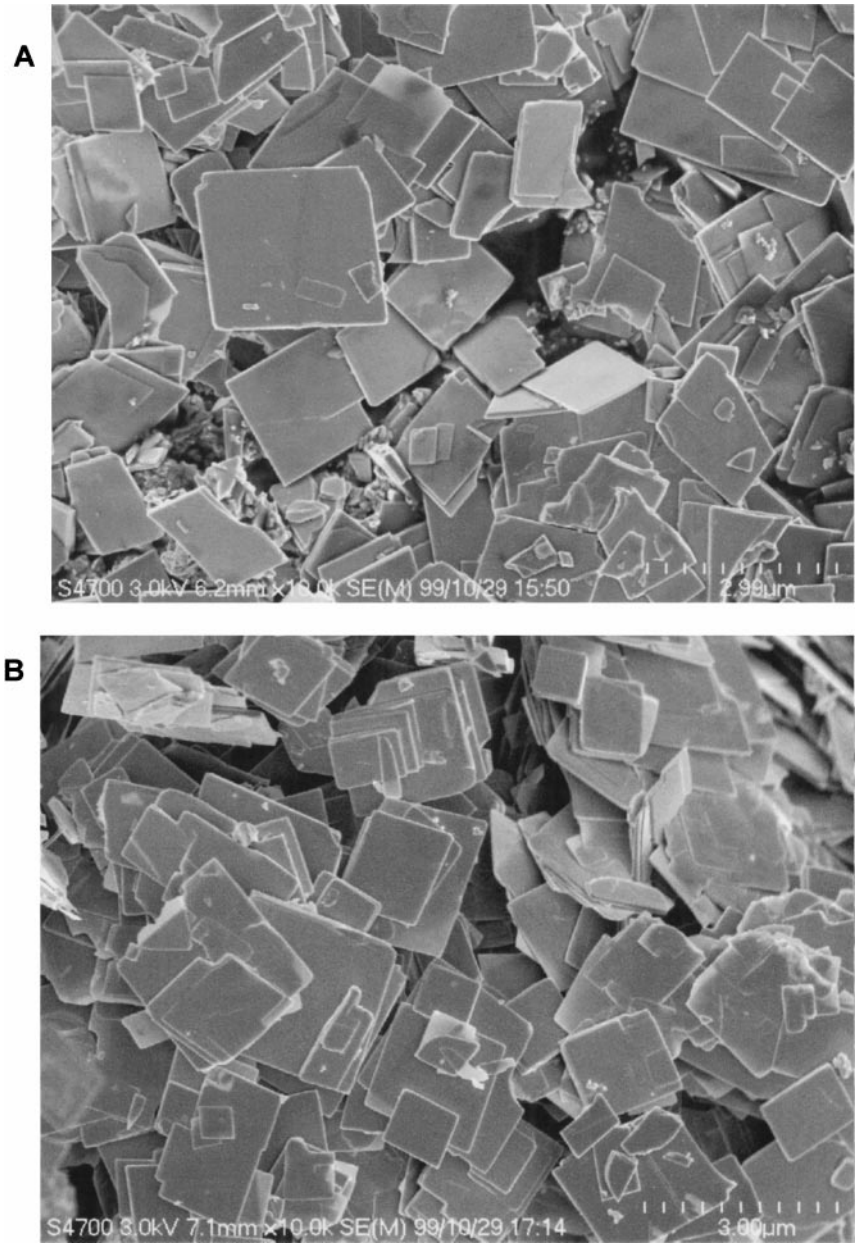

FIG. 8. Scanning electron micrographs of fresh $SbRe_2O_6$ (A), $SbRe_2O_6$ after the methanol oxidation at 573 K for 1 h (B), $SbRe_2O_6$ after the methanol oxidation at 593 K for 1 h (C), and $SbRe_2O_6$ after methanol oxidation at 673 K for 3 h (D). Scale bars are shown in each SEM photograph.

Figure 6 shows the Re 4*f* XPS spectra for the fresh $SbRe_2O_6$, and the $SbRe_2O_6$ samples after methanol oxidation at 573, 593, and 673 K. A small peak at 47.7 eV may be due to Re $4f_{5/2}$ for Re^{6+} species, while a strong peak at 42.3 eV may be referred to Re $4f_{7/2}$ for reduced Re species, likely Re^{4-5+} (38, 39). The most intense peak at about 44.7 eV is then considered as the sum of a Re $4f_{7/2}$ peak for Re^{6+} species and a Re $4f_{5/2}$ peak for Re^{4-5+} species. The Sb 4*d* and Sb $3d_{3/2}$ bands appeared at the binding energies of 34.4 and 539.7 eV, respectively, which are the values typical of Sb^{3+}. The observation of $Re^{4.5+}$ XPS peaks agrees with the chemical formula of $SbRe_2O_6$ containing Re ions with an oxidation state of 4.5+. The $SbRe_2O_6$ samples before and after methanol oxidation at 573 and 593 K exhibited no significant difference in the Re 4*f* XPS spectra (Figs. 6b and 6c). However, the $SbRe_2O_6$ sample after methanol oxidation at 673 K showed weakness in the Re 4*f* XPS peak intensities (Fig. 6d), indicating a change in the catalyst surface.

Figure 7 shows the Raman spectra for the fresh $SbRe_2O_6$ catalyst before exposure to methanol and the $SbRe_2O_6$ catalysts after methanol oxidation at 573, 593, and 673 K.

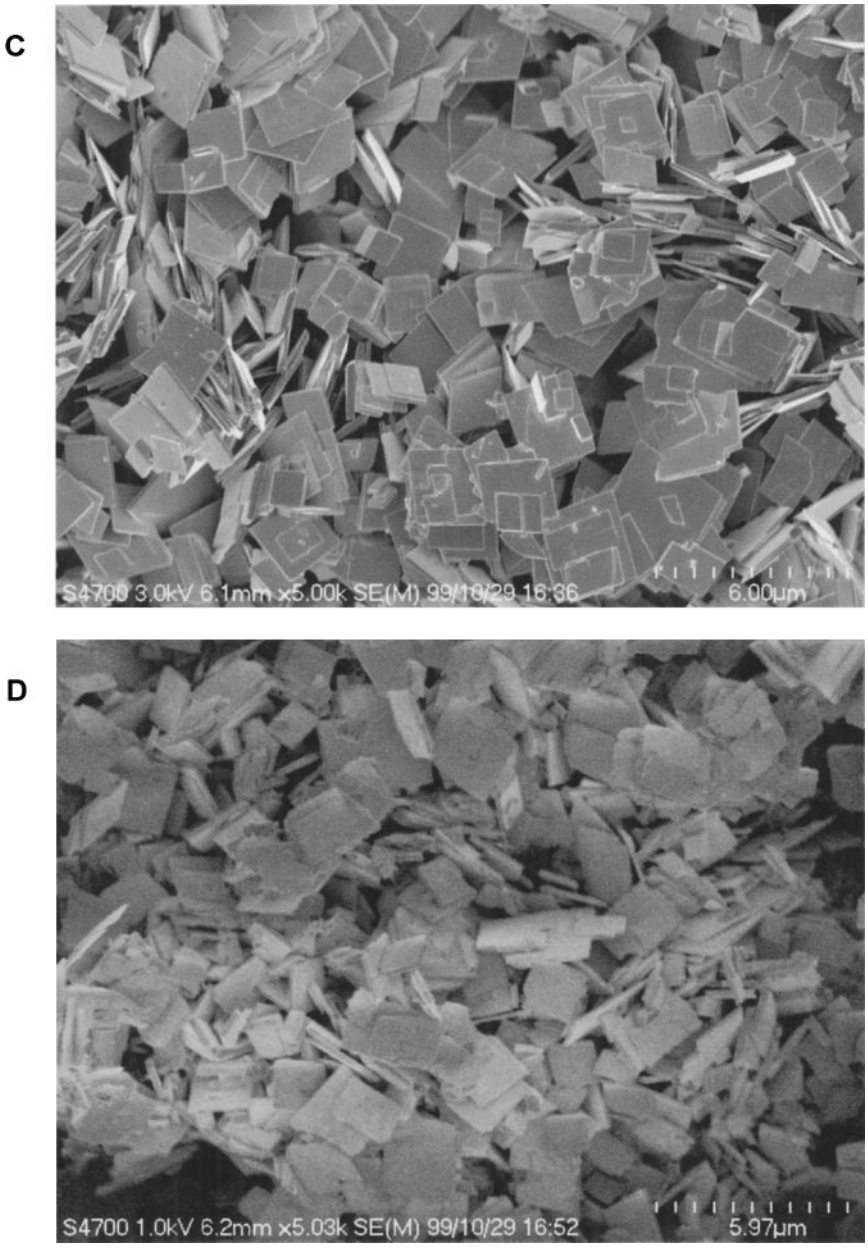

FIG. 8—*Continued*

The Raman spectrum for the fresh dehydrated $SbRe_2O_6$ catalyst showed bands at 152 sh, 171, 227 vs, 239 vs, 267, 282, 308, 347, 391, 416 sh, 525, and 756 cm^{-1}. After methanol oxidation at 573 and 593 K, there was no significant change in the bands. The $SbRe_2O_6$ sample after the catalytic methanol oxidation at 673 K, however, gave a new intensive Raman band at 201 cm^{-1}, accompanied by an increase in intensity of the broad band at 391 cm^{-1}.

Figures 8A–8D show the SEM micrographs for $SbRe_2O_6$ before and after the selective methanol oxidation at 573, 593, and 673 K, respectively. The fresh $SbRe_2O_6$ catalyst was composed of crystals possessing square basal faces with 0.5–3 μm in dimension and about 100 nm in thickness. The basal (100) faces were smooth and had sharp and regular edges. Also, after selective methanol oxidation at 573 and 593 K, the $SbRe_2O_6$ crystals exhibited almost the same morphology as the fresh sample. However, at 673 K the morphology granulated a little, though the crystals still maintained their regular shape.

3.6. TPD and TPR

The O_2 TPD spectra were obtained with the $SbRe_2O_6$ samples: (a) after pretreatment at 573 K in He and O_2-

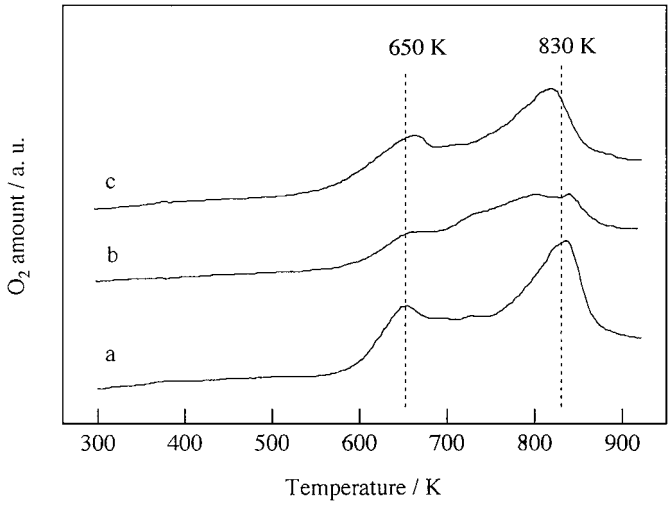

FIG. 9. O_2 TPD spectra for fresh $SbRe_2O_6$ (a), $SbRe_2O_6$ after the methanol oxidation at 573 K for 60 min in the absence of oxygen (b), and $SbRe_2O_6$ after the methanol oxidation at 573 K for 70 min in the absence of oxygen and then in the presence of oxygen for 10 min (c).

adsorption at 298 K, (b) after the methanol oxidation at 573 K in the absence of oxygen for 60 min, followed by cooling to 298 K in He, and (c) after the methanol oxidation at 573 K in the absence of oxygen for 60 min and next in the presence of oxygen ($He/O_2/MeOH = 79.3/9.7/10.0$ (mol%)) for 10 min, followed by cooling to 298 K in He. All the TPD experiments were carried out at a heating rate of 10 K/min. The results are shown in Fig. 9.

The TPD spectrum (Fig. 9a) showed the desorption peaks at about 650 and 830 K, which indicates the existence of two types of lattice oxygen species. The intensity of the two peaks decreased in similar manners after the catalytic oxidation of methanol at 573 K in the absence of gaseous oxygen for 60 min as shown in Fig. 9b. The two oxygen species that were exhausted in methanol oxidation were regenerated during catalytic methanol oxidation as evidenced in Fig. 9c.

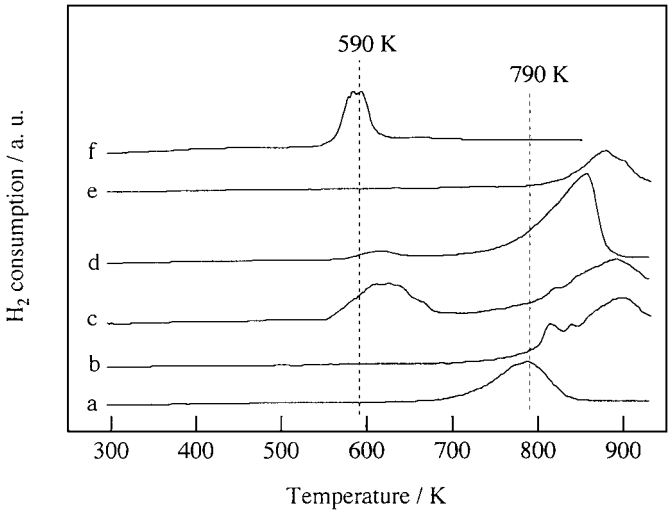

FIG. 10. TPR profiles for (a) fresh $SbRe_2O_6$, (b) fresh $Sb_4Re_2O_{13}$, (c) fresh $SbOReO_4 \cdot 2H_2O$, (d) 10 wt% Re_2O_7/Sb_2O_3, (e) Sb_2O_3, and (f) 10 wt% Re_2O_7/SiO_2.

Figure 10 shows the TPR spectra for $SbRe_2O_6$, $Sb_4Re_2O_{13}$, $SbOReO_4 \cdot 2H_2O$, 10 wt% Re_2O_7/Sb_2O_3, Sb_2O_3, and 10 wt% Re_2O_7/SiO_2. The $SbRe_2O_6$ gave one TPR peak at about 790 K, which was lower than the TPR peak for Sb_2O_3 but higher than that for the SiO_2-supported Re_2O_7. $Sb_4Re_2O_{13}$ and $SbOReO_4 \cdot 2H_2O$ showed totally different TPR features from that of the $SbRe_2O_6$. The reduction of $Sb_4Re_2O_{13}$ occurred above 800 K and $SbOReO_4 \cdot 2H_2O$ was reduced by two steps at about 610 K and above 800 K.

4. DISCUSSION

4.1. Catalytic Performances of Three Crystalline Sb–Re–O Compounds for the Selective Oxidation of Methanol to Methylal

Many catalysts have been screened to improve the performance for catalytic methanol oxidation, but little is known about the catalytic property of Sb–Re–O compounds. The catalytic methylal synthesis by methanol oxidation has been proposed on V/TiO_2 (2), V–Mo–O (5), $PMoH\text{-}5.75/SiO_2$ (6), Mo/MCM-41 (7), and electrocatalysts (9), but good achievements have not been reported so far (Table 1). As listed in Table 1, $SbRe_2O_6$ among the Sb–Re–O catalysts employed is the only catalyst that has excellent performance in the catalytic selective oxidation of methanol to methylal. The 2 mol% Mo/MCM-41 catalyst was reported to show high selectivity of 76.2% at a low conversion of 0.7% at 543 K, but rapid deactivation was serious due to a significant leaching of Mo species from MCM-41 (7). We found that the new $SbRe_2O_6$ catalyst is promising in the process for catalytic methylal synthesis from methanol with good selectivity of 92.5% (Table 1). The increase in the surface area of $SbRe_2O_6$ as well as the coverage of adsorbed methoxy species/methanol may improve the catalytic performance.

4.2. Structure of $SbRe_2O_6$ before and after the Catalytic Methanol Oxidation

The structure of $SbRe_2O_6$ consists of layers of the composition $[Re_2O_6]^{3-}$ and antimony ions connecting the layers, sharing all corners along the (100) axis, as shown in Fig. 11. The (100) plane tends to grow (Fig. 8). The formal oxidation states of rhenium and antimony in $SbRe_2O_6$ are 4.5+ and 3+, respectively. The mixed valent state of the rhenium makes Re–O bonds weaker and thus leads to a softer lattice (14).

The results of XRD, XPS, Raman, and SEM demonstrate that the structure of $SbRe_2O_6$ during the catalytic methanol

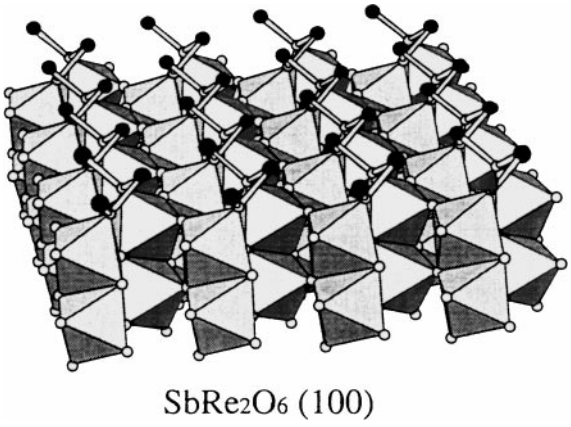

FIG. 11. A representative $SbRe_2O_6$ (100) plane; Re ions are located inside oxygen octahedra and Sb ions are shown with black scale. Small white circles are O^{2-} ions.

oxidation at the temperatures below 600 K remained unchanged. Another crystalline compound, $Sb_4Re_2O_{13}$, was also stable in the identical reaction conditions as characterized by XRD, XPS, and SEM, but it showed no catalytic activity for the selective methanol oxidation at 573 K (Table 1).

Although the Re 4*f* XPS binding energies reported for Re species so far are scattered in the literature (38, 39), the XPS spectra for $SbRe_2O_6$ in Fig. 6 indicate the presence of Re^{4-5+} species, which coincides with the chemical formula of $SbRe_2O_6$. The minor peaks for Re^{6+} species in Fig. 6 suggest that a part of Re^{4-5+} species at the catalyst surface is oxidized. It was observed that $SbRe_2O_6$ decomposed partly under the catalytic methanol oxidation at 673 K. At this reaction temperature a morphological change occurred as imaged by SEM (Fig. 8D). The XPS spectrum for the sample after the reaction at 673 K in Fig. 6d also indicates a surface change of the crystal, probably due to oxidation of Re species to Re^{7+} species on the surface of $SbRe_2O_6$. The amount of Re^{7+} species must be very small due to the volatile property of Re^{7+} oxide species (25), so that the Re^{7+} species was not definitely detected by XPS and Raman. The surface decomposition of $SbRe_2O_6$ and the volatilization of Re^{7+} oxide species caused a decrease in the intensity of the XPS Re 4*f* peaks. By comparison with the Raman bands for Sb_2O_4, the new Raman bands at about 201 and 391 cm^{-1} for the 673 K reacted sample are referred to as Sb_2O_4 formation, although Sb_2O_4 was not detected by XRD (Fig. 5d). Thus, the decomposition at the $SbRe_2O_6$ surface at 673 K may be postulated by Eq. [1]. The Re_2O_7 species *in situ* formed under methanol oxidation at O_2 partial pressures above 10 mol% in the reactant feed or at 673 K resulted in an increase in dimethyl ether formation due to the higher acidity of Re_2O_7 compared to that of the lower valent Re species.

$$4SbRe_2O_6 + 6O_2 \rightarrow 4Re_2O_7 + 2Sb_2O_4. \qquad [1]$$

4.3. Active Oxygen Species of $SbRe_2O_6$ for Selective Methylal Formation

When $SbRe_2O_6$ was exposed to methanol in the absence of oxygen, methylal was formed over 60 min and then the reaction products switched to H_2, CO_2, CH_4, and $HCOOCH_3$. The molecular ratio of $H_2/CO_2/CH_4$ was found to be approximately 2/1/1. The results suggest that the lattice oxygen in the crystalline $SbRe_2O_6$ was active and selective for the methanol oxidation to methylal:

$$3CH_3OH + [O] \rightarrow CH_2(OCH_3)_2 + 2H_2O. \qquad [2]$$

As shown in Fig. 4, a series of pulsed reactions of methanol in the absence of O_2 also indicates that lattice oxygen atoms of the $SbRe_2O_6$ catalyst contribute to the selective methylal synthesis. Figure 4 shows a plateau with the following notable decrease in the methanol conversion, which suggests that the surface lattice oxygen atoms consumed by the reaction with methanol can be replenished by bulk oxygen in $SbRe_2O_6$ at 573 K, though the amount of replenished oxygen atoms is not so much.

At the $SbRe_2O_6$ surface where the active lattice oxygen atoms had been consumed, formaldehyde produced by methanol dehydrogenation ($CH_3OH \rightarrow HCHO + H_2$) reacted with methanol to produce $HCOOCH_3$ by the dehydrogenative condensation (Eq. [3]) rather than the dehydrative condensation to form methaylal:

$$HCHO + CH_3OH \rightarrow HCOOCH_3 + H_2. \qquad [3]$$

Methyl formate was easily decomposed to CO_2 and CH_4 at the reduced catalyst surface. Thus, the overall stoichiometry of the surface reaction becomes $H_2/CO_2/CH_4 = 2/1/1$.

When O_2 was admitted into the reactant feed after the active lattice oxygen was exhausted, the methylal synthesis activity of $SbRe_2O_6$ was restored as shown in Fig. 3, which demonstrates that the active lattice oxygen species were regenerated by gaseous oxygen.

The TPD experiments in Fig. 9 reveal that there are two types of lattice oxygen atoms; one desorbs at 663 K and the other desorbs at 723 K. We may straightforwardly attribute these two lattice oxygen species to a Re oxide site and Sb oxide site in $SbRe_2O_6$ from the comparison with TPD of Re_2O_7/SiO_2 and Sb_2O_3 (not shown), respectively. These two TPD peaks decreased in intensity similarly after methanol oxidation in the absence of oxygen for 60 min (Fig. 9), which indicates that both of the two lattice oxygen species are responsible for selective methanol oxidation to methylal. When oxygen was introduced into the reactant feed, those decreased TPD peaks (Fig. 9b) developed again (Fig. 9c), which coincides with the results in Fig. 3.

The amount of the active lattice oxygen in $SbRe_2O_6$ can be estimated from the TPD results. Also, according to the reaction formula for the methylal formation from methanol (Eqs. [4] and 5), it is possible to calculate the amount of the

TABLE 2

The Amount of Active Lattice Oxygen Species for the Methanol Oxidation in $SbRe_2O_6$ Estimated from Reaction and TPD Data

	Active oxygen amount	
	$mmol/g_{-cat}$	$atom/m^2$
From the reaction (Fig. 3)	3.8×10^{-2}	2.4×10^{19}
From the TPD (Fig. 9)	2.4×10^{-2}	1.5×10^{19}

active lattice oxygen in Fig. 3 by curve simulation.

$$CH_3OH + [O] \rightarrow HCHO + H_2O \quad [4]$$

$$HCHO + 2CH_3OH \rightarrow CH_2(OCH_3)_2 + H_2O. \quad [5]$$

The calculated results from Figs. 3 and 9 are shown in Table 2. The difference between the two experiments may be due to the experimental errors since the amount of the active lattice oxygen was substantially small. The small amount of the active lattice oxygen in $SbRe_2O_6$ may be due probably to its low surface area of 1 m^2/g. The amount of the active oxygen atoms corresponds to $1.5–2.4 \times 10^{19}$ $atom/m^2$, which falls into the range of oxygen concentration at solid oxide surfaces (40).

4.4. Redox and Acid–Base Catalysis of $SbRe_2O_6$

From the mechanism of methanol oxidation reported on unsupported MoO_3 (41) and V–Ti–O systems (42), the first reaction step has been demonstrated to be the formation of methoxy species (42, 43) by dissociative adsorption of methanol on a dual acid–base site formed by accessible cation and surface oxygen ion. Further transformation of the adsorbed methoxy will depend on the redox property and acid–base strength of active centers on which it adsorbs. Desorption of the formaldehyde produced by dehydrogenation of the methoxy species is favored on weak acid sites more than on strong acid sites. If the acid sites are strong, the residence time of formaldehyde at the surface becomes long enough to form dioxymethylene species (42), and the dioxymethylene species can react with neighboring methoxy species and/or adsorbed methanol to form methylal (44). If both acidic and basic sites are too strong, the dioxymethylene species are oxidized to formates, which also react with methanol to form methyl formate molecules, or are further oxidized to carbon dioxides (42). If strong acid sites and very weak basic sites are present at catalyst surfaces, only dimethyl ether is formed (45). The present results indicate that $SbRe_2O_6$ can fit the requirements for both "redox" and "acid–base" catalyses for selective methanol oxidation to methylal at 573 K. Only the $SbRe_2O_6$ among the three crystalline Sb–Re–O compounds showed high performance for catalytic methylal synthesis. The oxidation state of Re oxide species and the stablization of the Re oxide species by the specific connection with the Sb oxide chains may be the key issues relevant to selective oxidation of methanol to methylal. The TPR results for $SbRe_2O_6$ in Fig. 10 showed that one reduction peak at 790 K, suggesting the occurrence of a distinct connection between the Re oxide and Sb oxide, which is different from the other two Sb–Re–O compounds. The well-organized bifunctions of the moderate redox and acidic property at the $SbRe_2O_6$ surface may be benefited from the specific valency and arrangement.

5. CONCLUSIONS

(1) The novel compound $SbRe_2O_6$ showed good performance with high selectivity of 92.5% for the catalytic methanol oxidation to methylal at 573 K. The reaction rate increased with increasing methanol partial pressure but was independent of oxygen partial pressure. The high selectivity to methylal was independent of the methanol concentration and the O_2 concentration (<10 mol%) in the reactant feed.

(2) No structural change in the bulk and surface of $SbRe_2O_6$ was observed during and after methanol oxidation at 573 K by means of XRD, Raman, XPS, and SEM. The $SbRe_2O_6$ surface benefited from the specific Re valency and arrangement provided high activity and selectivity to methylal.

(3) The pulse reactions showed that the lattice oxygen species in the $SbRe_2O_6$ contributed to the selective oxidation of methanol to methylal. The TPD experiments demonstrated that there existed two types of lattice oxygen, both being responsible for the methylal synthesis. The lattice oxygen atoms exhausted in the methylal formation were regenerated by gaseous O_2 during catalytic methanol oxidation.

ACKNOWLEDGMENT

This work has been supported by Core Research for Evolutional Science and Technology (CREST) of Japan Science and Technology Corporation (JST).

REFERENCES

1. Tatibouët, J. M., *Appl. Catal. A* **148**, 213 (1997).
2. Busca, G., Elmi, A. S., and Forzatti, P., *J. Phys. Chem.* **91**, 5236 (1987).
3. Ai, M., *J. Catal.* **77**, 279 (1982).
4. Arora, N., Deo, G., Wachs, I. E., and Hirt, A. M., *J. Catal.* **159**, 1 (1996).
5. Tatibouët, J. M., and Germain, J. E., *Bull. Soc. Chim. Fr. I* **9–10**, 343 (1980).
6. (a) Fournier, M., Aouissi, A., and Rocchiccioli-Deltchff, C., *J. Chem. Soc. Chem. Commun.* 307 (1994). (b) Rocchiccioli-Deltcheff, C., Aoussi, A., Launary, S., and Fournier, M., *J. Mol. Catal. A: Chem.* **114**, 331 (1996).
7. Shannon, I. J., Maschmeyer, T., Oldroyd, R. D., Sankar, G., Thomas, J. M., Pernot, H., Baalikdjian, J. P., and Che, M., *J. Chem. Soc. Faraday Trans.* **94**, 1495 (1998).

8. (a) Tatibouët, J. M., and Germain, J. E., *J. Catal.* **72**, 375 (1981). (b) Tatibouët, J. M., and Germain, J. E., and Volta, J. C., *J. Catal.* **82**, 240 (1983).
9. For example, Otsuka, K., and Yamanaka, I., *Appl. Catal.* **26**, 401 (1986).
10. Gaigneaux, E. C., Liu, H., Imoto, H., Shido, T., and Iwasawa, Y., *Top. Catal.* **11–12**, 185 (2000).
11. Liu, H., Gaigneaux, E. C., Imoto, H., Shido, T., and Iwasawa, Y., *J. Phys. Chem.* **104**, 2033 (2000).
12. Harrison, W. T. A., McManus, A. V. P., Kaminsky, M. P., and Cheetham, A. K., *Chem. Mater.* **3**, 1631 (1993).
13. Watanabe, H., and Imoto, H., *Inorg. Chem.* **36**, 4610 (1997).
14. Watanabe, H., Imoto, H., and Tanaka, H., *J. Solid State Chem.* **138**, 245 (1998).
15. Rae Smith, A. R., and Cheetham, A. K., *J. Solid State Chem.* **30**, 345 (1979).
16. Sleight, A. W., *Inorg. Chem.* **14**, 597 (1975).
17. Butz, A., Miehe, G., Paulus, H., Strauss, P., and Fuess, H., *J. Solid State Chem.* **138**, 232 (1998).
18. Moulijn, J. A., and Mol, J. C., *J. Mol. Catal.* **46**, 1 (1988). Mol, J. C., and Moulijn, J. A., "Advances in Catalysis" (D. D. Eley, H. Pines, and P. B. Weisz, Eds.), Vol. 24, p. 131. Academic Press, New York, 1975.
19. Olsthoorn, A. A., and Boelhouwer, C., *J. Catal.* **44**, 207 (1976).
20. Pecoraro, T. A., and Chianelli, R. R., *J. Catal.* **67**, 430 (1981).
21. Thomas, R., Van Oers, E. M., De Beer, V. H. J., Medema, J., and Moulijn, J. A., *J. Catal.* **76**, 241 (1982).
22. Blom, R. H., Kollonitsch, and Kline, C. H., *Ind. Eng. Chem.* **54**, 17 (1962).
23. Davenport, W. H., Kolonitsch, W., and Kline, C. H., *Ind. Eng. Chem.* **60**, 10 (1968).
24. Kim, D. S., and Wachs, I. E., *J. Catal.* **141**, 419 (1993).
25. Wang, C.-B., Cau, Y., and Wachs, I. E., *Langmuir* **15**, 1223 (1999).
26. Jehng, J.-M., Hu, H., Gao, X., and Wachs, I. E., *Catal. Today* **28**, 335 (1996).
27. Albonetti, S., Cavani, F., and Trifiro, F., *Catal. Rev.-Sci. Eng.* **38**, 413 (1996).
28. Nilsson, R., Lindblad, T., and Andersson, A., *J. Catal.* **148**, 501 (1994).
29. Zanthoff, H.-W., and Buchhloz, S. A., *Catal. Lett.* **49**, 213 (1997).
30. Grasselli, R. K., and Suresh, D. D., *J. Catal.* **25**, 272 (1972).
31. Genti, G., and Trifiro, F., *Catal. Rev.-Sci. Eng.* **28**, 165 (1986).
32. Berry, F. J., *Adv. Catal.* **30**, 97 (1981).
33. Inoue, T., Asakura, K., and Iwasawa, Y., *J. Catal.* **171**, 184 (1997).
34. Inoue, T., Asakura, K., and Iwasawa, Y., *J. Catal.* **171**, 457 (1997).
35. Inoue, T., Oyama, S. T., Imoto, H., Asakura, K., and Iwasawa, Y., *Appl. Catal. A* **191**, 131 (2000).
36. Yuan, Y., Liu, H., Imoto, H., Shido, T., and Iwasawa, Y., *Chem. Lett.* 674 (2000).
37. Castillo, R., Dewaele, K., Ruiz, P., and Delmon, B., *Appl. Catal. A* **153**, L1 (1997).
38. Cimino, A., De Angelis, B. A., Gazzoli, D., and Valigi, M., *Z. Anorg. Allg. Chem.* **460**, 86 (1980).
39. Shpiro, E. S., Avaev, V. I., Ryashentseva, M. A., and Minachev, Kh. M., *J. Catal.* **55**, 402 (1978).
40. Winter, E. R. S., *J. Chem. Soc. A* 2889 (1968).
41. Chung, J. S., Miranda, R., and Bennertt, C. O., *J. Catal.* **114**, 354 (1988).
42. Busca, G., *Catal. Today* **27**, 457 (1996).
43. Liu, Y. C., Griffin, G. L., Chan, S. S., and Wachs, I. E., *J. Catal.* **94**, 108 (1985).
44. Yang, T. J., and Lunsford, J. H., *J. Catal.* **103**, 55 (1987).
45. Chauvin, C., Saussey, J., Lavalley, J. C., Idriss, H., Hindermann, J. P., Kienneman, A., Chaumette, P., and Courty, P., *J. Catal.* **121**, 56 (1990).